Space Weather

RESEARCH ARTICLE
10.1029/2020SW002599

Beamline and Flight Comparisons of the ARMAS Flight Module With the Tissue Equivalent Proportional Counter for Improving Atmospheric Radiation Monitoring Accuracy

Brad "Buddy" Gersey[1,2], W. Kent Tobiska[1], William Atwell[1], Dave Bouwer[1], Leonid Didkovsky[1], Kevin Judge[1], Seth Wieman[1], and Richard Wilkins[3]

[1]Space Weather Division, Space Environment Technologies, Los Angeles, CA, USA, [2]NASA Center for Radiation Engineering and Science for Space Exploration, Prairie View A&M University, Prairie View, TX, USA, [3]Department of Electrical and Computer Engineering, Prairie View A&M University, Prairie View, TX, USA

Key Points:
- Measurements from a radiation detector based on the Teledyne uDOS001 were cross-calibrated to measurements from a TEPC microdosimer
- Results from parallel exposure of these instruments in 4 different radiation fields were utilized to create a new cross-calibration method
- Excellent agreement on seven airline flight measurements was found between the TEPC and the Teledyne uDOS001 using the new method

Correspondence to:
B. "B." Gersey,
bgersey@spacewx.com

Citation:
Gersey, B. "B.", Tobiska, W. K., Atwell, W., Bouwer, D., Didkovsky, L., Judge, K., et al. (2020). Beamline and flight comparisons of the ARMAS flight module with the tissue equivalent proportional counter for improving atmospheric radiation monitoring accuracy. *Space Weather*, *18*, e2020SW002599. https://doi.org/10.1029/2020SW002599

Received 31 JUL 2020
Accepted 28 OCT 2020
Accepted article online 20 NOV 2020

Abstract Ionizing radiation at aircraft and commercial suborbital spaceflight altitudes is driven by space weather and is a health concern for crew and passengers. We compare the response functions of two radiation detectors that were exposed to four different ground-based laboratory radiation fields as well as flown alongside each other on aircraft. The detectors were a tissue equivalent proportional counter (TEPC) and a Teledyne silicon micro dosimeter chip that was integrated into an Automated Radiation Measurements for Aerospace Safety Flight Module (ARMAS FM). Both detectors were flown onboard commercial and research aircraft. In addition, both detectors were exposed neutrons at the Los Alamos Neutron Science Center, protons at Loma Linda University Medical Center, ^{56}Fe particles at the NASA Space Radiation Laboratory, and also a gamma radiation source at Lawrence Livermore National Laboratory. The response of each of these instruments as well as derived dosimetric quantities are compared for each radiation exposure and the ratio for converting ARMAS absorbed dose in silicon to an estimated absorbed dose in tissue is obtained. This process resulted in the first definitive calibration of the silicon-based detector like ARMAS to TEPC. In particular, with seven flights of both instruments together, the ARMAS-derived dose in tissue was then validated with the TEPC-measured dose in tissue and these results are reported. This work provides a method for significantly improving the accuracy of radiation measurements relevant to human tissue safety using a silicon detector that is easy to deploy and can report data in real time.

1. Introduction

Aerospace safety has improved over the past decades in many areas including pilot training, flight weather specification, air drag efficiency, and avionics redundancy. However, long-term health effects from space weather due to ionizing radiation at higher altitudes and higher magnetic latitudes have not seen the same growth in safety awareness until very recently. Ionizing radiation exposure is a natural hazard faced by commercial aircrew, high-altitude pilots, frequent flyers, first trimester fetuses, and commercial space travelers. In this work we have significantly improved the accuracy of silicon-based radiation detection instrumentation through calibrations of measured dose in silicon converted to dose in tissue. These results will aid our understanding of the impacts from complex radiation fields upon humans.

Multiple sources of ionizing radiation contribute exposure in the aerospace environment from the Earth's surface into space. Galactic cosmic radiation (GCR) and solar energetic particles (SEPs) are the dominant ionizing radiation sources for travel in and above commercial aviation altitudes (Friedberg & Copeland, 2003, 2011). A large number of measurements used for postflight analysis have been made using Tissue Equivalent Proportional Counters (TEPCs) under GCR background conditions and not during major space weather SEP events (Beck et al., 1999, 2005, 2009; Dyer et al., 1990, 2009; Gersey et al., 2012; Getley et al., 2005, 2010; Hands & Dyer, 2009; Kyllönen et al., 2001; Latocha et al., 2007; Lindborg et al., 2004; Meier et al., 2009; Tobiska et al., 2014a, 2014b, 2015). Some of the measurements have included neutron flux and dose equivalent measurements with solid-state detectors (Dyer et al., 2009; Hands & Dyer, 2009; Lee et al., 2015; Ploc et al., 2013).

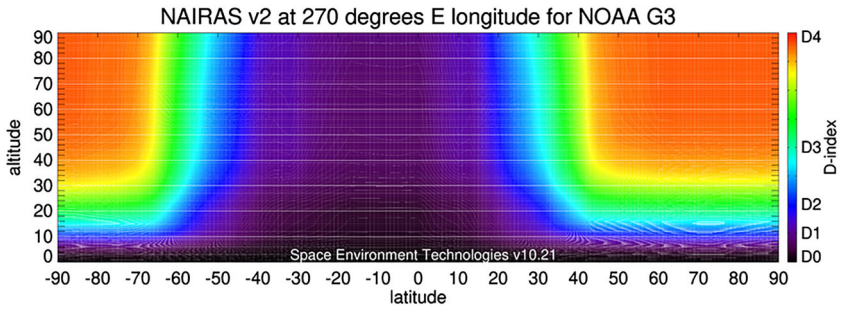

Figure 1. *NAIRAS* v1 radiation environment at longitude 270°E and NOAA G3 geomagnetic conditions shown by altitude (km) and geographic latitude. The D-index indicates severity of the tissue-relevant effective dose rates.

There are many modeling systems into which ionizing radiation data could be integrated, e.g., LUIN (O'Brien et al., 1996), CARI6PM (Friedberg et al., 1999; Friedberg & Copeland, 2003, 2011), FLUKA (Zuccon et al., 2001), QARM (Lei et al., 2006), AIR (Johnston, 2008), PARMA (Sato et al., 2008), AVIDOS (Latocha et al., 2009, 2014), NAIRAS (Mertens et al., 2013), PANDOCA (Matthiä et al., 2014), and KREAM (Hwang et al., 2014). Recent work by Joyce et al. (2014) utilized CRaTER measurements (Schwadron et al., 2012; Spence et al., 2010) in deep space to estimate dose rates through the Earth's atmosphere at a range of different altitudes down to aviation heights. Figure 1 shows an example of that radiation field from the NASA Langley Research Center's (LaRC) *Nowcast of Atmospheric Ionizing RAdiation System (NAIRAS)* v1 model (Mertens et al., 2013). Geographic latitude and altitude (km) are shown for a western hemisphere longitude at 270°E during NOAA G3 strongly geomagnetically active conditions. The D-index (Meier & Matthiä, 2014; Tobiska et al., 2017) relates the severity of effective dose rates for humans in an atmospheric radiation field. "D" in D-index stands for "dose" and the black, purple, and blue colors indicate lower effective dose rates while green-yellow show moderate effective dose rates and orange-red represent elevated effective dose rates. The D-index was developed to provide warnings of elevated radiation levels. It is based on the radiation exposure from solar particle and radiation belt precipitation added to background GCRs. It is created from the effective dose rate, which can be derived from either measurements or models. The D-index range from D0 to D8 covers a wide range of radiation exposures at aviation altitudes. D0, D1, and D2 levels are for quiet space weather conditions. D3 is for elevated exposure from more particles coming into the atmosphere and can be used by air traffic management to trigger a radiation warning. D4 and higher indicate radiation alerts can occur infrequently but during large solar events.

All longitudes are provided through the public access ARMAS app available in Apple's App store.

GCRs are produced outside the solar system and mostly consist of energetic protons that penetrate through the heliosphere; they are modulated by the strength of the Sun's interplanetary magnetic field (Simpson, 1983). SEPs come from solar activity, i.e., coronal mass ejections related to flaring events or from interplanetary magnetic field shocks (Gopalswamy, 2004; Reames, 2013). A third radiation source has been identified and likely originates from the wave-particle interaction in the Van Allen radiation belts leading to precipitated charged particles (Tobiska et al., 2016, 2018); this is an area of continued active research.

The primary ionizing dose in the aerospace environment, which can be altered with both the composition of the terrestrial atmosphere and the dynamic variability of the Earth's magnetosphere, produces highly variable secondary and tertiary ionizing radiations. These particularly cause concern for human health and vehicle avionics (IEC 62396–1, 2016) in higher altitude and higher latitude aviation as illustrated in Figure 1.

Radiation detection in space and aboard aircraft is a challenge due to the complexity of the primary and secondary radiation environment. Ground-based experiments are required to test and benchmark the response of existing and new detectors in order to gain insight into the operational efficacy of their measurements. Two radiation detectors were utilized in this study. We performed a cross-calibration followed by measurement comparisons in four ground-based beamline experiments and seven aircraft flights. The two detectors were a *TEPC*, the community's "gold standard" for tissue-relevant radiation detection (Badhwar et al., 1992, 1995), and a detector based on the Teledyne micro dosimeter chip called *Automated Radiation Measurements for Aerospace Safety Flight Module (ARMAS FM)*. In this study both of these radiation detectors were flown together onboard aircraft to perform measurements of the ambient radiation field while in flight.

Both detectors were also exposed to four different radiation fields during ground-based experiments. A direct comparison of the absorbed dose, D, measured by each detector during the ground-based experiments and aircraft flights were then made. Further insight was obtained concerning a normalization method for converting dose in silicon, D (Si) (measured by the *ARMAS FM*), to dose in tissue, D (Ti) (measured by the *TEPC*), using results from these ground-based experiments. The seven flights were conducted across the midcontinental United States to capture changes in cutoff rigidities at flight altitudes.

The rationale for making the *ARMAS-TEPC* calibration, with validation, was to develop a system that could give the quality of information provided by *TEPC* but without the penalties of instrument fragility, heavy weight, and inability to conduct real-time monitoring, as is the case with *TEPC*. The *TEPC* data analysis is a complex process and the advantages of the *ARMAS FM* are superior for robust data streaming its real-time results, low size/weight/power, and ease of operation. Our results improve the accuracy for determining absorbed dose, D (Ti), and dose equivalent, H, using the *ARMAS FM* detector for nominal exposure conditions. Ground-level events (GLEs) and large solar particle events (SPEs) are not included in this analysis and require modeling as well as measurements from a larger body of work. This accuracy also lays a solid foundation for using silicon-based calibrated, automated detectors to provide a continuous flow of aerospace radiation environment information. The information is particularly useful for monitoring regulatory compliance with guidelines by international organizations such as the International Civil Aviation Organization (ICAO). The most important dosimetric parameters for this monitoring include the total absorbed dose (and rate) in tissue as well as the total dose equivalent (and rate).

2. Instrumentation and Experimental Facilities

Two radiation detectors were exposed to four different ground-based radiation fields. Their characteristics are described as are the ground-based experiment facilities.

2.1. Radiation Detection Instrumentation

2.1.1. TEPC

The *TEPC* used in the ground-based beamline experiments is an active radiation detector similar in design and identical in function to the *TEPC* used aboard the space shuttle to provide energy loss spectra for crew dosimetry (Badhwar, 1997; Badhwar et al., 1992; Badhwar, Cucinotta, et al., 1994). It has an active volume that is a right circular cylinder 1.78 cm long and 1.78 cm in diameter. The walls of this cylinder are fabricated from tissue equivalent A-150 plastic and are 1.9 mm thick. The cylinder is enclosed in stainless steel walls of 0.89 mm thickness. The active volume is then enclosed in an aluminum cylinder, which measures 2 in. in diameter and is 12 in. long. The active volume of the *TEPC* is filled with low-pressure tissue equivalent (TE) gas (propane) to simulate tissue material as a right circular cylinder with 2 μm diameter and length (International Commission on Radiation Units and Measurements, 1983). An anode wire runs the length of the cylinder and is kept at a potential of 670 V relative to the cylinder walls.

When energy is deposited in the *TEPC* active volume, charge is collected at the anode wire and is processed by a preamplifier. The signal then moves from the preamplifier to two shaping amplifiers. These two shaping amplifiers have a difference in gain of approximately a factor of 50. After shaping amplification, the two signals are converted to a digital pulse height by means of an analog to digital converter (ADC). These pulse height signals are then stored on a flash-ROM card for later analysis. Pulse height information as well as instrument health and status are time-stamped and stored to flash-ROM in 1-min increments. Health and status information for the *TEPC* include reporting of instrument temperature, voltage, and current draw for each minute of operation.

During data analysis, the pulse height signals are combined to form a pulse height distribution. This distribution is then calibrated and converted into a lineal energy (y) deposition distribution (N(y) vs. y). The *TEPC* is capable of measuring a lineal energy deposition spectrum ranging from 0.4–1,250.0 keV μm^{-1}. The y spectrum is used to determine the absorbed dose to tissue from the radiation incident upon the *TEPC*. By making the assumption that y is equal to the linear energy transfer (LET) of the radiation field, this same spectrum is used to approximate the LET spectrum of the incident radiation (Badhwar, Konradi, et al., 1994; Badhwar et al., 1995, 1996). This LET spectrum is then used to calculate absorbed dose, D, dose equivalent, H, and an average quality factor, Q, of the radiation in tissue (Johnson et al., 1993). Absorbed Dose in Silicon, D (Si), is the amount of energy absorbed by silicon per unit mass. This fundamental radiation measurement

Figure 2. SolarMetrics/SET HAWK *TEPC*.

quantity for Absorbed Dose in silicon has units of Gray (Gy). Absorbed Dose in Tissue, D (Ti), is the amount of energy absorbed by human tissue per unit mass. This fundamental radiation measurement quantity for Absorbed Dose in tissue has units of Gray (Gy). Dose Equivalent, H, is the radiation quantity used to report a person's exposure for regulatory, medical, and scientific purposes. Regulatory limits are expressed in units of Dose Equivalent. Dose Equivalent is calculated by multiplying the Absorbed Dose (D) times the Average Quality Factor (Q) ($H = D \times Q$). Units for Dose Equivalent are reported in Sieverts (Sv). Average Quality Factor, Q, scales the exposure in a specific radiation field to the potential biological risk. The dose equivalent from the radiation field is determined using the values of the absorbed dose and the average quality factor. Using the time-stamp information, the time profile of dose and dose equivalent is then calculated.

The calculated quantities of absorbed dose, D (Ti), dose equivalent, H, and an average quality factor, Q, of the radiation in tissue are shown in Equation 1. The calculation of absorbed dose (International Commission on Radiation Units and Measurements, 1983), D, in J kg^{-1}, is

$$D = \frac{\sum \varepsilon \cdot N(\varepsilon) d\varepsilon}{\rho_g \cdot V_g}, \quad (1)$$

where ε is the energy deposited in the *TEPC* (Joules) as derived from a lineal energy spectrum. $N(\varepsilon)d\varepsilon$ is the number of particle events depositing energy ε. ρ_g is the density of the TE gas in the *TEPC* gas cavity (kg cm^{-3}). V_g is the volume of the *TEPC* gas cavity (cm^3). The SI unit of absorbed dose is Gray (Gy), which is equal to 1 J kg^{-1}. We note that the unit for absorbed dose in the United States is called the Rad and 1 Gy is equal to 100 Rad.

The quality factor, Q, is defined as a dimensionless scaling parameter that is a function of the LET of incident radiation into tissue produced by the absorbed dose (International Commission on Radiological Protection, 1991). The dose equivalent, H, is the product of Q and D at a specific point in tissue (International Commission on Radiation Units and Measurements, 1993). This is shown in Equation 2 and is in SI units of Sievert (Sv), where 1 Sv is also equal to 100 REM.

$$H = Q \bullet D. \quad (2)$$

The dose equivalent, H, is used in radiation protection standards for humans and we further note that while Gy is an absorbed dose, Sv is an absorbed dose that takes into account the type of radiation in tissue since some types of radiation are more damaging than others, thus leading to the term "dose equivalent." Q is the scaling factor that transforms absorbed dose to dose equivalent.

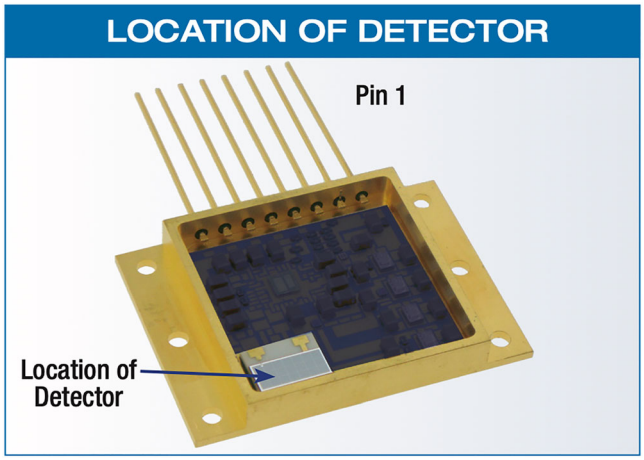

Figure 3. Teledyne uDOS001.

The *TEPC* used for measuring the radiation field onboard aircraft flights, results of which are reported in section 3, is owned by SolarMetrics and flight managed by SET (Figure 2). It has an active volume that is different in size and shape from the shuttle-style *TEPC* used in the beamline experiments conducted by Prairie View A&M University (PVAMU) for many years (Gersey et al., 2004; Gersey, Aghara, et al., 2007, Gersey, Sodolak, et al., 2007) but is virtually identical in all other ways including electronics, data management and storage, data analysis. The shuttle-style TEPC has been used in beamline experiments by this team and it has provided reliable and consistent microdosimetry measurements in a multitude of different radiation fields (Gersey, Aghara, et al., 2007; Gersey, Sodolak, et al., 2007; Gersey et al., 2004, 2012). The *TEPC* used on aircraft flights is denoted

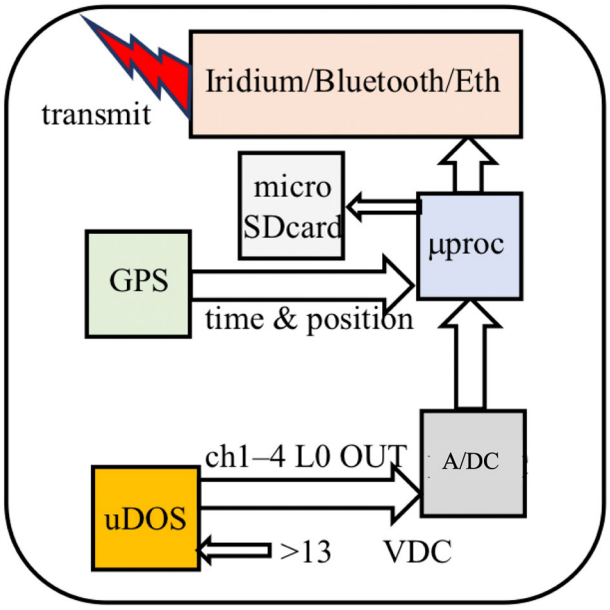

Figure 4. *ARMAS* concept.

as a HAWK style and its active volume is a spherical cavity 12.57 cm in diameter with a wall (comprised of A-150 tissue equivalent plastic) 0.241 cm thick; its active volume is filled with low-pressure propane gas to simulate a 2-µm diameter sphere (*TEPC* Technical Manual, Far West Technologies).

2.1.2. Automated Radiation Measurements for Aerospace Safety Flight Module (ARMAS FM)

The *ARMAS* radiation measurement flight system uses Teledyne micro dosimeters (uDOS001, Figure 3) developed by The Aerospace Corporation, manufactured under license by Teledyne, and first used by the CRaTER experiment on the Lunar Reconnaissance Orbiter (Mazur et al., 2011; Spence et al., 2010). The uDOS001 directly measures total ionizing dose (TID) absorbed by an internal silicon test mass; this is also called absorbed dose in silicon, D (Si). The entire chip size is $3.56 \times 2.54 \times 0.10$ cm. By accurately measuring the energy absorbed from heavy ions, alphas, protons, neutrons, electrons, and gamma rays (γ rays), an estimate of the absorbed dose in silicon is made. The micro dosimeter provides repeatable measurements of TID in silicon over a wide range of energies (60 keV to >175 MeV) and operating temperatures (−30 to +40°C). In *ARMAS*, the instrument is typically operated at aircraft cabin temperatures (15–25°C); for environments colder than −15°C, passive thermal insulation is used. The micro dosimeter operates from input power voltages >13 VDC. Figure 4 is a diagram of the *ARMAS* instrument measurement concept and Figure 5 shows an *ARMAS* Flight Module 7 (FM7) with Bluetooth capability that is used in business jet and commercial aerospace vehicles.

The accumulated dose is reported via three DC linear and one pseudo-logarithmic output channels in units of millivolts, giving a dose resolution of 14 µrads and a measurement range exceeding 100 krads. Each channel (ch1–ch4) has a resolution of 256 steps, i.e., values of 0–255, and when a lower channel rolls over to 0 the next higher channel is incremented by 1. Level 0 (L0) raw data are reported as the output of the four channels, each having a value of 0–255. In addition to the uDOS001 and ADC providing ch1–ch4 information, a microprocessor (µproc) is used to accumulate the absorbed dose measurements over time; the integration time varies but 10 s is used operationally. Along with an input GPS signal for time and position, the output L0 information is both stored on an internal micro SD card data logger as well as sent externally via one of several systems. Depending upon the configuration of the specific *ARMAS* instrument, the L0 and GPS information may be sent via Iridium satellite link, Bluetooth to a paired iPhone or iPad via the *ARMAS* app, Ethernet, USB, RS232, or I^2C. Measured D (Si) is continuously downloaded from the instrument to the SET *ARMAS* servers via WiFi or Iridium downlink.

Figure 5. *ARMAS FM7* instrument.

2.2. Ground-Based Experimental Facilities

There were four different facilities utilized in this study and each facility provided a different and distinctly well-characterized radiation field. These four radiation fields were chosen to represent important components of the complex mix of radiation found in the atmosphere and in space. The two radiation detectors were exposed to radiation at these facilities under identical conditions so that a meaningful comparison of the measured absorbed dose could be made.

2.2.1. Los Alamos Neutron Science Center (LANSCE) Neutron Source

The LANSCE 30L beamline (Irradiation of Chips Electronics (ICE) House) delivers high energy and relativistic neutrons from 1–800 MeV in energy. The neutron energy spectrum on this beamline is very similar to the secondary neutron energy spectrum found in the upper atmosphere (Figure 6). One hour of exposure in the neutron beamline is equivalent to 30,000 h at 12 km (39,370 ft.).

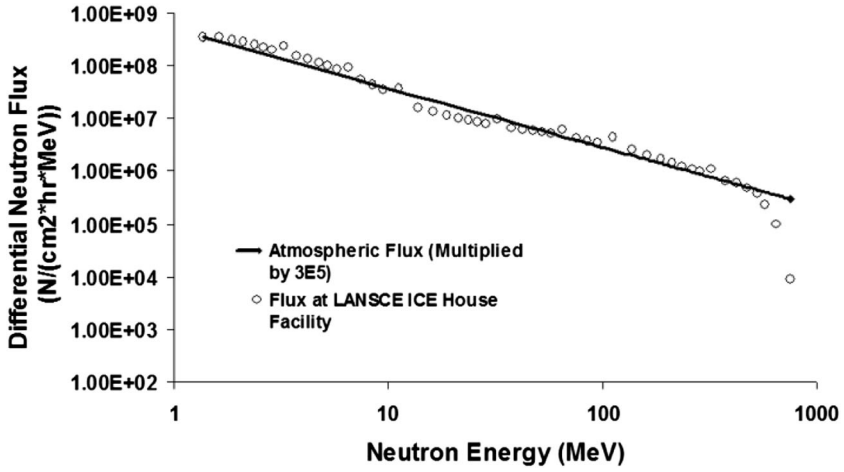

Figure 6. Differential neutron flux at LANSCE ICE House facility and neutron flux found in the atmosphere at an altitude of 12,000 m multiplied by 3×10^5 (Gersey et al., 2003).

The neutron beam at the ICE House is produced by a spallation reaction caused by 800 MeV protons striking a tungsten target. The ICE House beam line is located approximately 20 m from the spallation source and is 30° to the left (30L) of the incident proton beam direction. Both the neutron energy spectrum and the total number of neutrons during each experimental exposure in the ICE House are measured using a fission chamber detector coupled with a Time Of Flight (TOF) analysis system (Wender et al., 1993).

A laser system was used to align both the *TEPC* and the *ARMAS FM* detectors in the ICE House neutron beam line as shown in Figure 7. After each detector was exposed to the neutron beam for a given period of time, analysis of the data from each detector was performed resulting in a determination of the total measured absorbed dose. The resulting total absorbed dose for each experimental exposure was then divided by the total number of neutrons per cm^2 for each exposure; this information is provided by the ICE House fission chamber detector system. This normalization procedure allowed a meaningful comparison of results between the two detectors and between the same detector exposed for different lengths of time (Gersey, Aghara, et al., 2007; Gersey et al., 2003).

2.2.2. Loma Linda University Medical Center (LLUMC) Proton Synchrotron

LLUMC is capable of producing high energy protons at energies of interest to the aerospace radiation dosimetry community, e.g., 75–250 MeV. The Horizontal Beam Line (HBL) treatment bay beam line was utilized as the experimental area to expose the two detectors to high energy protons. In this study a 175 MeV proton beam was utilized due to the fact that this energy of protons is prevalent during normal solar activity and during SPEs, especially in the secondary radiation environment. Protons with these energies are also found in the upper atmosphere and can penetrate to internal organs. The *TEPC* and the *ARMAS* were exposed to the 175 MeV proton beam separately and the absorbed dose measurements for each detector were determined during post experimental analysis.

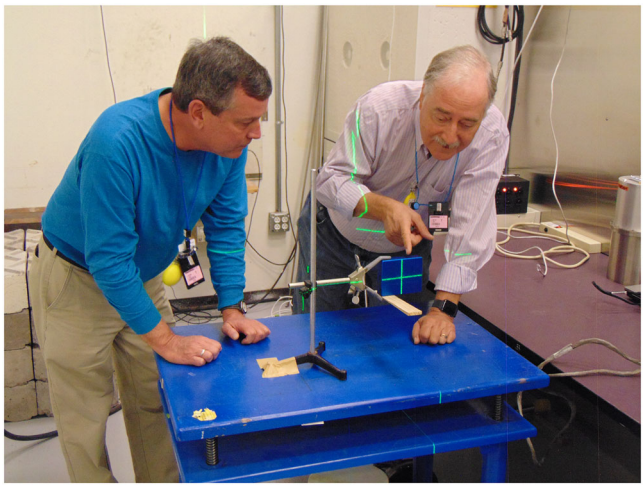

Figure 7. B. Gersey and K. Tobiska using a laser to center the *ARMAS FM* detector in the ICE House neutron beamline.

The LLUMC synchrotron facility did not have a method to determine the total number of protons delivered to the experimental area during each exposure. Instead, the facility was able to provide a measurement from a foil detection system upstream of the experimental area (denoted Tic1 foil in this study). The number of Tic1 foil counts measured by this system during any given experimental exposure was directly proportional to the number of protons per cm^2 delivered by the synchrotron. The number of Tic1 foil counts measured during each experimental exposure of the *TEPC* and *ARMAS FM* was therefore used to normalize the absorbed dose measurements of these devices for comparative purposes.

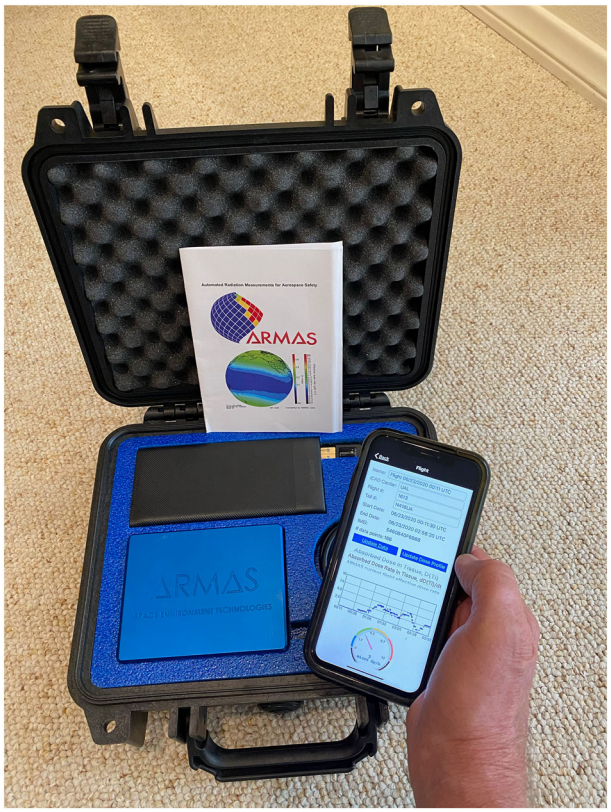

Figure 8. *ARMAS FM7* instrument in flight carrying case with a paired *ARMAS* app.

Figure 9. *TEPC* instrument in flight carrying case.

2.2.3. Brookhaven National Laboratory's NASA Space Radiation Laboratory (NSRL) Particle Beam

NSRL is a facility capable of delivering protons and heavy ions at energies found in both the Galactic Cosmic Radiation (GCR) and SEP spectrum in space and at the top of the atmosphere. The species of ions that the NSRL facility is capable of delivering range from H up to ^{197}Au. The maximum energy that each ion can be delivered at is species dependent and range from 400–2,500 MeV/nucleon. At NSRL the energy and species of radiation chosen for this study was 350 MeV/nucleon ^{56}Fe ions. This energy and species of particle was chosen to represent the High Z and Energy (HZE) portion of the GCR and SEP spectrum. The absorbed dose measured by each detector after exposure to the ^{56}Fe beam was normalized by the number of ^{56}Fe ions per cm^2. The number of ^{56}Fe ions per cm^2 delivered during each exposure was determined using a scintillation counter positioned in the particle beam next to the radiation detectors.

2.2.4. Lawrence Livermore National Laboratory (LLNL) Gamma Ray Source

LLNL provided a ^{60}Co 1.25 MeV NIST traceable gamma ray source for this study. These energetic photons are a component of the radiation field in the upper atmosphere. The *ARMAS* and the *TEPC* were placed in a low scatter facility 200 cm away from the ^{60}Co source during exposure. Further details of this LLNL irradiation facility may be found in Straume et al. (2016). Once the measured absorbed dose was determined for the *ARMAS* and the *TEPC*, the results were normalized by the elapsed time for each exposure.

2.3. Instrumentation Protocol for Aircraft Flight Exposures

The detectors used for in-flight dosimetry comparisons were simultaneously flown aboard both commercial and research aircraft. In the research vehicle, which was an ER-2 from Armstrong Flight Research Center (AFRC) in Palmdale California, the *TEPC* and *ARMAS* were mounted in their own experiment racks. On commercial aircraft the two instruments were carried in their own cases in the overhead bin on the aircraft. Figures 8 and 9 show the method of carrying the *ARMAS* and *TEPC* instruments, respectively, during the flight tests. In addition, Figure 8 shows the *ARMAS* app running on an iPhone that is paired to the *ARMAS* instrument. Each instrument carried its own power supply for the flight and was not connected to aircraft systems.

3. *ARMAS FM* Calibration to *TEPC* Utilizing Ground-Based Experimental Results

External to the *ARMAS FM*'s microprocessor, the *ARMAS* v10.21 algorithms on the ground server transform the Level 0 (L0) millivolt data into L1 D (Si), which is converted to Rad (0.01 Gray) and then to SI units of micro Gray (μGy) using the conversion Equation 3.

$$\mathrm{D\ (Si)} = (\mathrm{ch1 \bullet 14.0}) \times 10^{-2} + (\mathrm{ch2 \bullet 3.6}) \times 10 + (\mathrm{ch3 \bullet 0.9}) \times 10^{4}, \quad (3)$$

where ch1, ch2, and ch3 are the first three channels of the Teledyne uDOS001. The pseudo-logarithmic output in channel 4 is not used in the data calculation. The L1 measurements of D (Si) are combined with time tag plus location information. The L2 absorbed dose rate, dD (Si)/dt in μGy h^{-1}, is the time derivative of the L1 TID. Operationally, a 10 data record time step, dt, is used to calculate a rate.

Table 1
LANSCE 1–800 MeV Neutrons

Detector	Absorbed dose (D) μGy/neutron
ARMAS	3.422 E-07 absorbed dose (D_{Si}) μGy/neutron
TEPC	6.310 E-06 absorbed dose (D_{Ti}) μGy/neutron
Ratio	18.439 × ARMAS $D_{Si} = D_{Ti}$

Both the D (Si) and dD (Si)/dt, which are the fundamental measurements by *ARMAS*, are converted to D (Ti) and dD (Ti)/dt for absorbed dose rate in tissue. This is accomplished by comparing the D (Si) from *ARMAS* to the D (Ti) of *TEPC*. A combination of ground-based beamline and flight experiments with both *ARMAS* and *TEPC* allowed the calibration then validation between dD (Si)/dt and dD (Ti)/dt. The methodology for representing dose rate in tissue using silicon-based detectors has three steps: (1) conduct the beamline experiments in known, single-species radiation fields and compare the two detectors to find the scaling ratio from dose in silicon to dose in tissue; (2) develop an algorithm to account for weighting the contributions from each species in mixed radiation fields at unique altitudes and magnetic field cutoff rigidities; and (3) validate the D (Si) to D (Ti) conversion by comparing derived *ARMAS* D (Ti) with measured *TEPC* D (Ti) using real flight data.

3.1. Step 1

Starting with the beamline experiments, we compared the absorbed dose in silicon from *ARMAS* with the *TEPC* absorbed dose in tissue. Tables 1–4 show the details for each of the beamline experiments. In the table title each facility, the species measured, and the energies used in the experiment are identified. In each row is presented the *ARMAS* detector's normalized absorbed dose in silicon in that facility's beamline, the *TEPC* detector's normalized absorbed dose in tissue in the same beamline, and the scaling ratio required to convert the *ARMAS* dose in silicon to dose in tissue for that unique source. We use one table for each of the beamline facilities, which have been described above.

A key comparison element is that the only parameter we need to determine the conversion is the ratio between the detectors' normalized observations; they use common units that are unique for different facilities. For example, LANSCE units of measurement were μGy/neutron, LLUMC were μGy/Tic1foil, NSRL were μGy/particle/cm^2, and LLNL were μGy/h. Since only ratios were needed for scaling *ARMAS* dose in silicon to *TEPC* dose in tissue using detectors in the same beamline with common units, this simplified our analysis. The silicon-to-tissue ratio vector for weighting each radiation source is defined in Equation 4 as

$$\mathbf{R}_i = [8.390,\ 8.390,\ 18.439,\ 9.629,\ 1.200,\ 1.200,\ 1.200] \bullet C0, \tag{4}$$

for ^{56}Fe ions, alphas, neutrons, protons, gamma rays, electrons, and pions-muons, respectively. C0 = 0.91 • (1/7), where 1/7 normalizes the ratios for seven fractional sources dependent on cutoff rigidity, R_c, whose units are GV, and altitude, z, with km used here. The factor of 0.91 is the scaling compensation for 9% unknown error in the calibration of D (Si) to D (Ti) that comes from unmeasured and uncalibrated contributions from known physical processes, including energy from unmodeled electrons and pions-muons. The elements of the $\mathbf{R}_i$ ratio vector are composed of the ratios listed in Tables 1–4 converting dose in silicon to dose in tissue. Alpha particles are set to ^{56}Fe ion values while electrons as well as pions-muons are set to gamma ray photon values since these have not been separately measured but have similar (International Commission on Radiological Protection, 1991) weighting values as described below.

3.2. Step 2

Because dose in silicon to dose in tissue ratios for single species radiation fields have now been calculated, the task is to account for the proper mixing of these sources in radiation fields as they occur in the natural atmospheric environment. Using the information for the fractional source contributions based on flight altitude, z, radiation source, i, and a cutoff rigidity, R_c, a tensor is formed, $\mathbf{GV}_{z,i,Rc}$, such that a subset can then be iteratively extracted as a vector based on the *i*th values at an altitude and a unique cutoff rigidity. This vector is called $\mathbf{G}_i$ and is multiplied by the $\mathbf{R}_i$ vector at each flight altitude then summed to create a source weighted factor at a flight altitude and cutoff rigidity unique to that flight. This value, called C3 in the *ARMAS* algorithm, is shown in Equation 5.

$$C3 = \sum (\mathbf{R}_i \times \mathbf{G}_i). \tag{5}$$

The C3 scale factor is used for the entire flight. By using the single flight value at altitude maximum, the operational complexity of calculating C3

Table 2
LLUMC 175 MeV Protons

Detector	Absorbed dose (D) μGy/Tic1foil
ARMAS	0.003 absorbed dose (D_{Si}) μGy/Tic1foil
TEPC	0.033 absorbed dose (D_{Ti}) μGy/Tic1foil
Ratio	9.629 × ARMAS $D_{Si} = D_{Ti}$

Table 3
NSRL 350 MeV/Nucleon ^{56}Fe Ions

Detector	Absorbed dose (D) μGy/particle/cm^2
ARMAS	0.022 absorbed dose (D_{Si}) μGy/particle/cm^2
TEPC	0.187 absorbed dose (D_{Ti}) μGy/particle/cm^2
Ratio	8.390 × ARMAS D_{Si} = D_{Ti}

introduced during long flights crossing many altitudes and cutoff rigidity levels can be more easily managed as a simplifying approach to calculate flight dose parameter information. Uncertainty at any specific location is, of course, increased. However, the uncertainty is still small since flights typically spend most of their time at cruise (maximum) altitudes and radiation at lower altitudes during take-off and landing is not only much less but occurs for a shorter duration.

The *ARMAS* D (Si) and dD (Si)/dt are multiplied by the C3 scale factor to get L2 dosimetric parameters of D (Ti) and dD (Ti)/dt that now correspond to the *TEPC* measured values as shown in Equations 6a and 6b. Across the entire *ARMAS* database, for all 751 flights at the time of this paper, the median of all the C3 scale factors is 1.42774 ± 0.0822 (1-σ). The variation across all flights had a maximum value in C3 of 1.52702 and a minimum value of 0.96557.

$$D\ (Ti) = D\ (Si) \bullet C3, \tag{6a}$$

$$dD\ (Ti)/dt = D\ (Si)/dt \bullet C3. \tag{6b}$$

Therefore, with the calculation of D (Ti) and dD (Ti)/dt, the L3 dosimetric parameter of dose equivalent rate, dH/dt in μSv h^{-1}, can be calculated and is shown in Equations 7a and 7b.

$$H = D\ (Ti) \bullet Q_{SET}, \tag{7a}$$

$$dH/dt = dD\ (Ti)/dt \bullet Q_{SET}, \tag{7b}$$

where the Quality factor at the geophysical location of measurement, Q_{SET}, is derived. Q_{SET} uses a fit to the results of Q vs. cutoff rigidity (R_c) by the method in Figure 10 using Equation 8. Q_{SET} has a RMS 1-σ uncertainty of ±12% due to (i) ± 10% uncertainty for modeling R_c with the planetary geomagnetic index, Kp; (ii) ±3.6% uncertainty from *TEPC*-measured, same altitude polar to equatorial estimates (Burda et al., 2013); and (iii) ±5% uncertainty in a polynomial fit to Burda data shown in Figure 10 and Equation 8.

$$Q_{SET} = 2.175 - 0.066 \bullet R_c + 0.001 \bullet R_c^2. \tag{8}$$

The method using Equation 8 to estimate Q_{SET} was verified by TEPC measurements of Q (Gersey et al., 2012). However, one of the largest uncertainty terms in the *ARMAS* v10.21 algorithm is for determining the correct Quality factor.

A next L3 dosimetric parameter of ambient dose equivalent rate, dH*(10)/dt in μSv h^{-1}, is calculated in Equation 9 by multiplying dH/dt with scaling factors to compare favorably with *NAIRAS* v1 data for commercial aviation altitudes. Ambient Dose Equivalent, H*(10), is a quantity developed for operational field measurements. It reports the average absorbed dose from all radiation at a depth of 10 mm inside a tissue equivalent material such as a human torso phantom. Units for Ambient Dose Equivalent are reported in Sieverts (Sv). *NAIRAS* v1 calibration was based on the RaD-X balloon mission results (Mertens et al., 2016).

$$dH^*(10)/dt = dH/dt \bullet C2 \bullet C1N. \tag{9}$$

Here C2 = 1.90 and is the conversion to ambient dose equivalent and C1N = 0.81 is the additional scaling considering dose at a depth of 10-cm in a phantom torso (C. Mertens, private communication).

Table 4
LLNL 1.25 MeV ^{60}Co Gamma Rays

Detector	Absorbed dose rate (dD/dt) μGy/h
ARMAS	26.936 absorbed dose rate (dD_{Si}/dt) μGy/h
TEPC	32.330 absorbed dose rate (dD_{Ti}/dt) μGy/h
Ratio	1.200 × ARMAS D_{Si} = D_{Ti}

The final L4 dosimetric parameter of effective dose rate, dE/dt in μSv h^{-1}, is calculated in Equation 10. Effective Dose, E is derived using a mathematical system that weights the H_T (Dose Equivalent received by each separate organ tissue (T) in the human body) by a unique weighting factor (W_T). This weighting factor takes into account the specific sensitivity of each organ to different types of radiation. When the product of these calculations for each organ are summed, the total value is the Effective Dose,

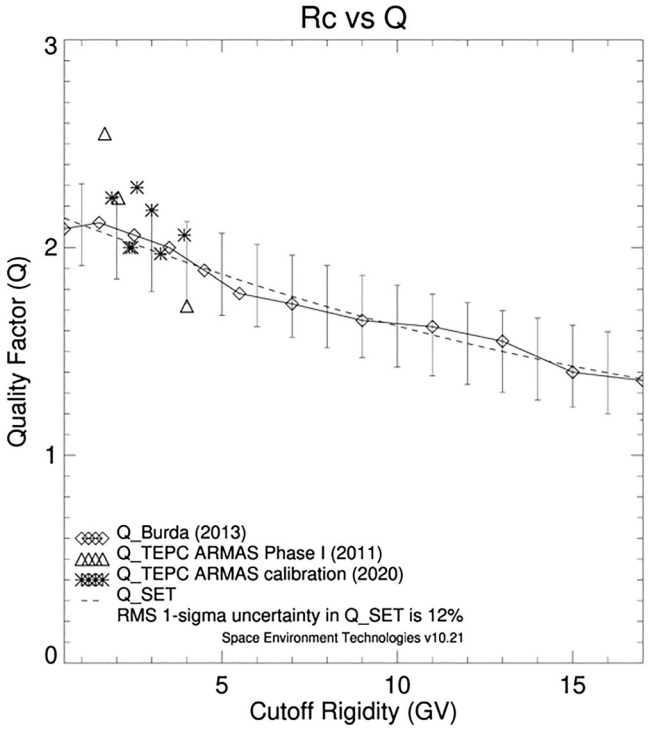

Figure 10. Q_{SET} as the dashed line fit to the Burda measurements of Quality factor (Q) (diamonds with error bars), verified with Gersey *TEPC* data (triangles) (Tobiska et al., 2016), and shown with TEPC Q values from Table 5 (asterisks).

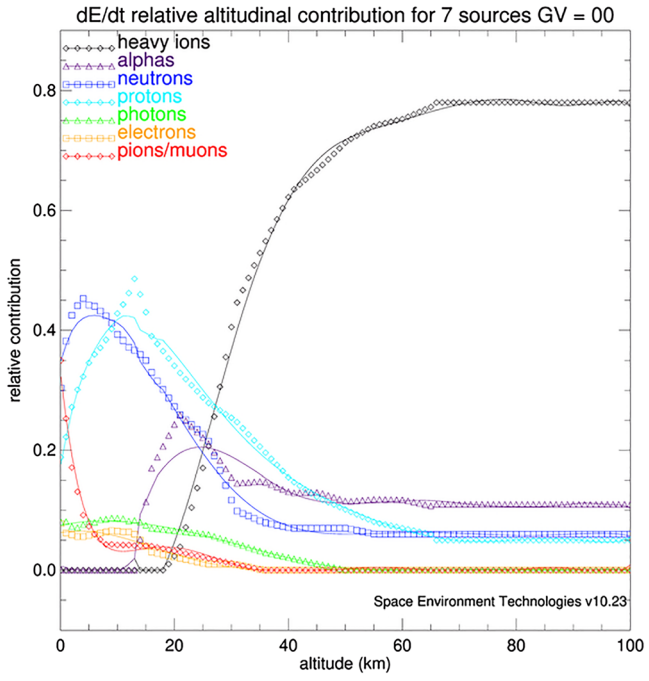

Figure 11. Relative contribution by altitude for seven sources at a cutoff rigidity for the polar region with a value of GV = 0.

E. Calculating the Effective Dose is especially useful in determining radiation risk for individuals that have received partial body irradiations. For individuals receiving uniform full body irradiations (nonlocalized partial body irradiations), the risk calculated by Effective Dose is the same as that measured in Dose Equivalent. Units for Effective Dose are reported in Sieverts (Sv).

$$dE/dt = \left(\mathbf{F}_{(z,\,i)} \times \mathbf{W}_i\right) \bullet dH/dt \bullet C4, \tag{10}$$

by considering the combined effects of (i) source particle fractional contribution to effective dose at altitude and cutoff rigidity and (ii) the source radiation weighting factor (International Commission on Radiological Protection, 1991). We note that $\mathbf{F}_{(z,i)}$ is an array of the fractional contributions by altitude, z, and source species, i, at a specific cutoff rigidity (R_c); $\mathbf{W}_i$ is an array of ICRP radiation weighting factors by seven sources = [20, 20, 5, 5, 1, 1, 1] where the International Commission on Radiological Protection (1991) values for weighting are heavy ions (e.g., ^{56}Fe) and alphas = 20, neutrons and protons = 5, and photons, electrons, pions-muons = 1; and C4 = 0.44, which is the weighted scaling to *NAIRAS* v1 effective dose rate mostly formed by the incoming GCR environment.

Previous calibration discussions for the *ARMAS* system have been described (Tobiska et al., 2016, 2019) and have been encapsulated in *ARMAS* algorithms preceding v10. The earlier work (Tobiska et al., 2016) calibrated dD (Ti)/dt and dH/dt dosimetric quantities in the *ARMAS* system to the *RaD-X* balloon mission results (Mertens, 2016; Mertens et al., 2016) and dH*(10)/dt as well as dE/dt to the *NAIRAS* v1 physics-based radiation model. A summary of that calibration work by Tobiska et al. (2019) provides a discussion of comparative measurements between *ARMAS* and *TEPC* between 2011 and 2019.

In this paper we have accomplished more than an updated calibration. We demonstrate the first definitive measurements, in a controlled laboratory environment, of ratios that justify the fit of the *ARMAS FM* to *TEPC* for absorbed dose in tissue. In developing this methodology, we have taken the ground-based dosimetry calibration ratios and considered the weighting ratios for atmospheric species and the weighting ratios for species' tissue damage. In the next section, we validate the *ARMAS* calibration to *TEPC* measurements for the dD (Ti)/dt and dH/dt parameters in the actual atmosphere modulated by space weather with real flight data. For dH*(10)/dt and dE/dt we continue to use the method of calibrating to *NAIRAS* v1 (Mertens et al., 2016). We do not consider shielding by the *ARMAS FM* housing thickness (100 mil = 0.254 cm aluminum) nor the thickness of the airplane walls, where we use 5.3 g cm^{-2} aluminum and 3.0 g cm^{-2} high-density polyethylene (HDPE) (personal communication, March 2010, W. Atwell). Shielding studies with *NAIRAS* v2 will be done in a separate paper.

The *ARMAS* v10.21 data processing software made improvements from earlier versions by specifying the relative contribution at altitude for seven sources (heavy ions, alphas, neutrons, protons, photons, electrons, pions-muons) as used in Equation 10. These sources have a dependence on altitude and cutoff rigidity; examples are shown for cutoff rigidity value in units of GV = 0 (magnetic pole; Figure 11) and GV = 17 (magnetic equator; Figure 12). The fractions of source contributions for a given altitude

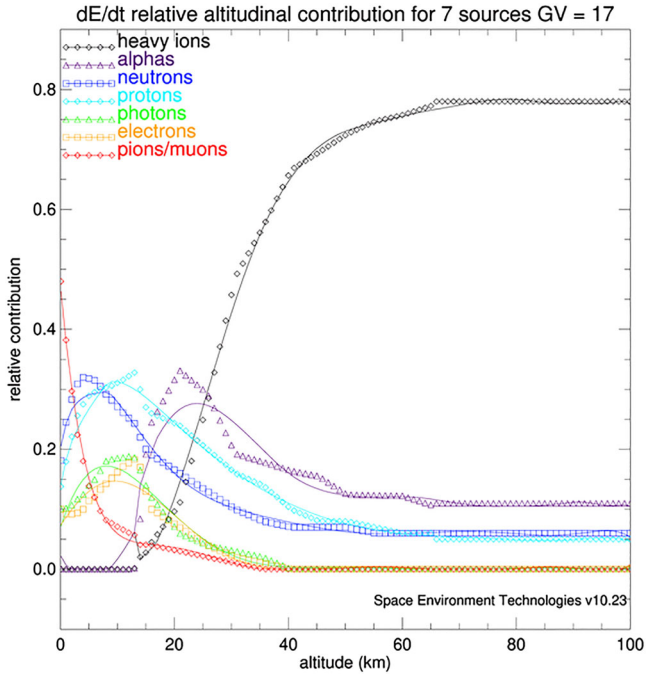

Figure 12. Relative contribution by altitude for seven sources at a cutoff rigidity for the equatorial region with a value of GV = 17.

slice sum to 1.0. In this analysis, we have not included any dependencies in the GCR modulation due to both solar cycle and Forbush decreases. These are important and need to be addressed in future work. The data points between 0 and 13 km were taken from Matthiä et al. (2014) while data points between 14 and 100 km were taken from Norman et al. (2016). Fitted curves to the datapoints are obtained for the effective dose fractional contributions and we use the smooth analytic curves for the *ARMAS* dose calculations. Separate from those works, alphas and heavies were separated to match the International Commission on Radiological Protection (1991) weighting and, in operations, altitudes greater than 100 km are set to 100 km values. The dose calculations in ARMAS to an altitude of 100 km is important since this marks the top of the atmosphere for suborbital commercial rockets at the present time and SET supplies dose data to those types of organizations in flight support. The Equation 10 based on Figures 11 and 12 allows for a seamless dose exposure environment from the surface of the Earth to the top of the atmosphere.

3.3. Step 3

The final task is to validate flight values for *ARMAS* with *TEPC* in the actual atmosphere. We have selected seven flights for this comparison where both instruments flew together, mostly in the configuration of Figures 8 and 9 described above. It was noted above that a key scaling factor in this work, C3, converting dose in silicon to dose in tissue was a median value (1.42774 ± 0.0822) across all 751 flights in the ARMAS database. The seven comparison flights were part of this calculation, comprising ~1% of the data. The exact C3 values for each flight are listed in Table 5 and are all well within the ±1-σ bounds.

Previously, Tobiska et al. (2019) showed a comparative example of absorbed dose rates for two of the commercial flights used here, i.e., Los Angeles–Denver (20 May 2018 at 11.3 km; Figure 13) and Denver–Los Angeles (23 May 2018 at 11.6 km; Figure 14) during very similar quiet geomagnetic conditions. Flight altitudes and locations come from ADS-B uncorrected pressure altitude flight records that are distributed by FlightAware. These figures have been updated using the new dose rates from the *ARMAS* v10.21 algorithm. In the top panel of each figure the ARMAS in flight absorbed dose rate, dD (Ti)/dt, is shown vs. time. Error bars of the data are provided and the plot legend provides the numerical value of the RMS uncertainty

Table 5
TEPC and ARMAS v10.21 Comparison on Same Continental U.S. Flights

Detector	Date	Flight	Absorbed dose rate dD (Ti)/dt (μGy/h)[a]	Dose equivalent rate dH/dt (μSv/h)[a]	Q (unitless)[a]	C3 value during flight (median = 1.42774 ± 0.0822)
TEPC	20 May 2018	LAX–DEN	2.37 ± 0.06	4.69 ± 0.21	1.97 ± 0.04	–
ARMAS	20 May 2018	LAX–DEN	2.40 ± 0.61	4.73 ± 1.20	1.97 ± 0.03	1.429
TEPC	23 May 2018	DEN–LAX	2.51 ± 0.06	5.48 ± 0.25	2.18 ± 0.04	–
ARMAS	23 May 2018	DEN–LAX	2.39 ± 0.80	4.75 ± 1.59	1.99 ± 0.03	1.424
TEPC	27 March 2019	LAX–DEN	2.44 ± 0.06	5.59 ± 0.25	2.29 ± 0.05	–
ARMAS	27 March 2019	LAX–DEN	2.40 ± 1.04	4.83 ± 2.09	2.01 ± 0.04	1.429
TEPC	06 April 2019	DEN–LAX	1.49 ± 0.04	3.34 ± 0.15	2.24 ± 0.04	–
ARMAS	06 April 2019	DEN–LAX	1.24 ± 0.48	2.55 ± 0.98	2.06 ± 0.03	1.475
TEPC	14 July 2019	LAX–IAD	2.51 ± 0.06	5.56 ± 0.25	2.22 ± 0.04	–
ARMAS	14 July 2019	LAX–IAD	2.48 ± 1.09	5.28 ± 2.32	2.13 ± 0.05	1.478
TEPC	19 July 2019	IAD–LAX	2.42 ± 0.06	5.30 ± 0.24	2.19 ± 0.04	–
ARMAS	19 July 2019	IAD–LAX	2.48 ± 1.01	5.17 ± 2.10	2.08 ± 0.05	1.478
TEPC	09 September 2015	Palmdale	4.77 ± 0.21	9.82 ± 0.73	2.06 ± 0.06	–
ARMAS	09 September 2015	Palmdale	4.60 ± 1.02	8.89 ± 1.97	1.93 ± 0.01	1.370

[a]Average *TEPC* and median *ARMAS* values at cruising altitudes; all flights are commercial except Palmdale ER-2.

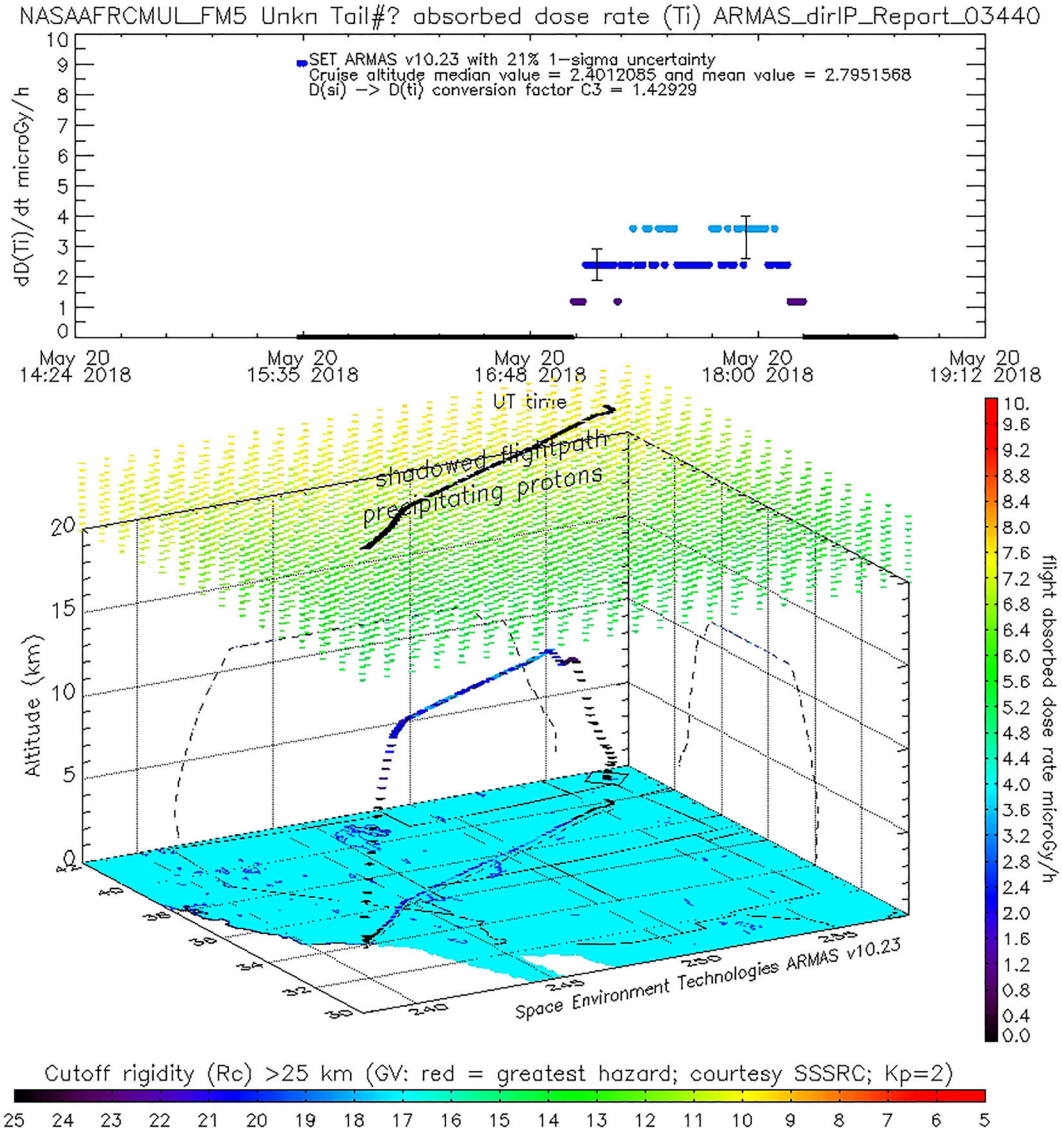

Figure 13. ARMAS LAX–DEN flight 20 May 2018.

(±21%), the median value at cruise altitude of dD (Ti)/dt, and the C3 conversion factor for that flight as described in Equations 5, 6a, and 6b. The bottom panel of each figure shows the 3-D graphical latitude, longitude, and altitude representation of the flight path with the diamond symbol at the termination of the flight. The flight is shadowed on each axis and on both the top and bottom of the figure. Above 20 km on the grid, the notional proton precipitation is shown and color-coded with the cutoff rigidity color bar at the bottom of the plot. The size of the proton representation is proportional to the climatological flux on those field lines. The intent of this proton "ceiling" is to graphically represent the change in cutoff rigidities along the shadowed flight path. Cutoff rigidity modeling is from an updated algorithm provided by Shea and Smart (Shea et al., 1987).

Table 5 is similar to the Table 1 in Tobiska et al. (2019) but updated for *ARMAS* v10.21 results; it also includes additional flights where *TEPC* and *ARMAS* were flown together. The absorbed dose rate, dD (Ti)/dt (μGy/h), dose equivalent rate, dH/dt (μSv/h), and Quality Factor, Q (unitless), for the cruising flight altitudes in Table 5 demonstrate an excellent comparison between the average *TEPC* and median *ARMAS* v10.21 values. The *TEPC* average cruise values are within ±1σ RMS standard deviation of the *ARMAS* median values.

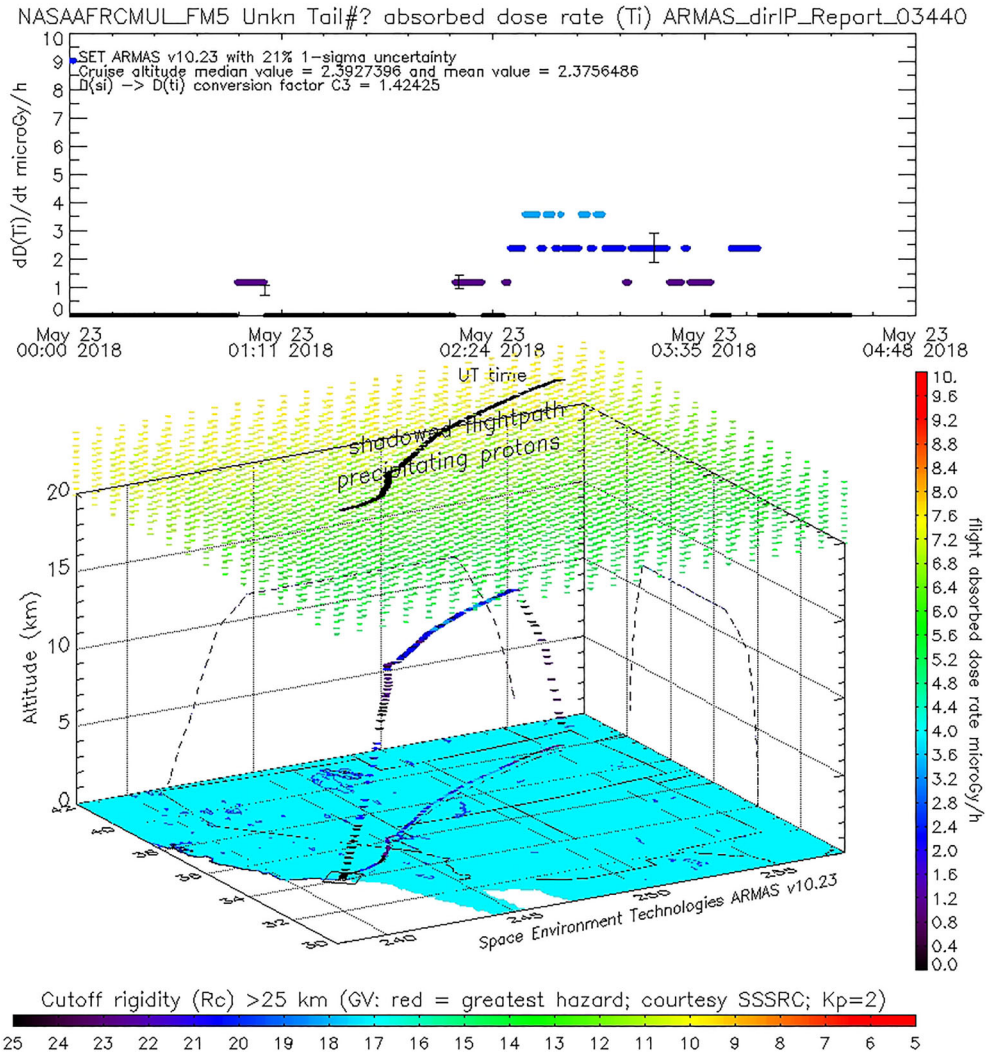

Figure 14. ARMAS DEN–LAX flight 23 May 2018.

Independent methods of determining Q were used where *TEPC* provides a measurement while *ARMAS* makes a calculation based on cutoff rigidities as summarized in Equation 8 and discussed in Tobiska et al. (2016, 2019). The total ±1σ RMS standard deviation in the *ARMAS* dose rate dD (Ti)/dt is ±21% and the ±1σ RMS standard deviation for the dose equivalent rate dH/dt is ±24%. The uncertainty in the ambient dose equivalent rate dH*(10)/dt is ±26% and the uncertainty in the effective dose rate dE/dt is ±26%. The terms included in these error calculations are described previously in detail by Tobiska et al. (2016) although we have improved their error estimations in the *ARMAS* v10.21 algorithm. The uncertainties used in this paper are identified in Table 6.

Typically, minimum cruise altitude values of *ARMAS* match very well with *NAIRAS* v1, which is realistic since *NAIRAS* v1 presents climatology based mostly on the GCR source component. There are very few SEP events in *NAIRAS* v1, which would be present during GLEs and perhaps subGLEs. These events require further study. Radiation belt particles are not modeled. If there is excess radiation not modeled by *NAIRAS* v1, as we suspect with bremsstrahlung gamma rays due to precipitated high-energy radiation belt particles, then *ARMAS* accurately captures that additional dose above the *NAIRAS* v1 GCR background. Radiation belt particle precipitation to mesospheric altitudes and subsequent gamma ray bremsstrahlung photon production is an area of active research and is not discussed in this paper.

Table 6
Uncertainties Used in This Calibration for ARMAS

ID	Long descriptor	Uncertainty ±1σ	Comment
R_{01}	RMS1sigmaTeledyne	20.0	Teledyne published uncertainty (Mazur et al., 2011)
R_{02}	RMS1sigmaARMASL1	2.66559	Mean RMS total absorbed dose (Si) uncertainty through time using paired instruments on same flights
R_{03}	RMS1sigmaARMASL2	4.68215	Mean RMS absorbed dose rate (Si) uncertainty using paired instruments on same flights
R_{04}	RMS1sigmaDRcalc	5.0	Dose rate calculation uncertainty
R_{05}	RMS1sigmaKp	10.0	Estimated uncertainty for Rc model with Kp
R_{06}	RMS1sigmaBurda	3.6	Polar to equatorial uncertainty (Burda et al., 2013)
R_{07}	RMS1sigmafit	5.0	Polynomial fit to Burda uncertainty, Figure 10
R_{08}	RMS1sigmaRaDX	2.0	RaD-X conversion between TID and TEPC uncertainty (Mertens et al., 2016)
R_{09}	RMS1sigmaNamb	abs(C2–1.0)*0.1*100	Normalized ambient dose equivalent uncertainty
R_{10}	RMS1sigmaSiTi	0.0	Si to Ti conversion uncertainty estimate [known]
R_{11}	RMS1sigmaQ	$(R_{05}^2 + R_{06}^2 + R_{07}^2)^{0.5}$	Total uncertainty in Q
R_{12}	RMS1sigmaL2Si	$(R_{01}^2 + R_{02}^2 + R_{03}^2 + R_{04}^2)^{0.5}$	Total uncertainty in D (Si)
R_{13}	RMS1sigmaL2Ti	$(R_{01}^2 + R_{02}^2 + R_{03}^2 + R_{04}^2 + R_{10}^2)^{0.5}$	Total uncertainty in D (Ti)
R_{14}	RMS1sigmaL2	$(R_{01}^2 + R_{02}^2 + R_{03}^2 + R_{04}^2 + R_{08}^2)^{0.5}$	Total uncertainty in D
R_{15}	RMS1sigmaL3dH	$(R_{01}^2 + R_{02}^2 + R_{03}^2 + R_{04}^2 + R_{05}^2 + R_{06}^2 + R_{07}^2 + R_{10}^2)^{0.5}$	Total uncertainty in dH/dt
R_{16}	RMS1sigmaL310	$(R_{01}^2 + R_{02}^2 + R_{03}^2 + R_{04}^2 + R_{05}^2 + R_{06}^2 + R_{07}^2 + R_{09}^2 + R_{10}^2)^{0.5}$	Total uncertainty in dH*(10)/dt
R_{17}	RMS1sigmaL4dE	$(R_{01}^2 + R_{02}^2 + R_{03}^2 + R_{04}^2 + R_{05}^2 + R_{06}^2 + R_{07}^2 + R_{08}^2 + R_{09}^2 + R_{10}^2)^{0.5}$	Total uncertainty in dE/dt

4. Conclusions

The need for monitoring the radiation environment in aerospace domains relevant to commercial aviation and commercial suborbital travel comes as there is a move toward regulatory compliance for radiation hazard management using guidelines by international organizations such as ICAO. The most important dosimetric parameters for this monitoring include the total absorbed dose (and rate) in tissue as well as the total dose equivalent (and rate). Because the *TEPC* is a large, weighty instrument not suitable for making real-time measurements, and whereas operational systems need automated, calibrated real-time data feeds, we were motivated in this work to calibrate the *ARMAS* system to *TEPC* for the benefit of operational users requiring monitoring compliance. To improve ability for this monitoring compliance, we present, in this study, the silicon-based *ARMAS FM* cross-calibration with a *TEPC* that converts dose measured in silicon to dose measured in tissue using four ground-based beamline experiments with species-dependent scaling ratios. Seven aircraft flights were used to validate the derived *ARMAS* dD (Ti)/dt and dH/dt in comparison with the *TEPC* measured parameters. In addition, we describe a methodology for normalizing these ratios between different experimental facilities and species. We also provide a methodology for considering mixed radiation fields in the natural atmosphere environment using all the dominant source species that are present. These fractions of species in these mixed radiation fields are dynamic and vary with altitude as well as magnetic field cutoff rigidity, which is continually perturbed by the solar wind.

In the first of three steps, i.e., the development of scaling ratios, both *ARMAS* and *TEPC* detectors were exposed to high energy and relativistic neutrons at the Los Alamos Neutron Science Center (LANSCE), high energy protons at Loma Linda University Medical Center (LLUMC), high energy ^{56}Fe particles at the NASA Space Radiation Laboratory (NSRL) Brookhaven National Laboratory, and a ^{60}Co gamma ray source at Lawrence Livermore National Laboratory. These four radiation sources were chosen to represent the main primary and secondary components of the mixed radiation field that occurs naturally from 8 to 100 km altitude.

In the second of three steps, results from the ground-based exposures were used to develop a normalization methodology using a species-dependent scaling ratio that includes consideration of species' fractional contributions at altitude and modulated by cutoff rigidity. This allowed the determination of D (Ti) from the

Acknowledgments
The authors acknowledge support for the *ARMAS* and *RADIAN* programs from the NASA SBIR Phase I and Phase II program contracts NNX11CH03P and NNX12CA78C, the NASA AFRC Phase III contracts NND14SA64P and NND15SA55C, the South Korean Space Weather Center matching funds for SBIR Phase IIE, the NASA FO *ARMAS-Hi* contract NND17AP04A, the NASA SBIR *ARMAS-DM* contract 80NSSC18P2111, and the NASA LWS *RADIAN* grant 80NSSC18K0187. The Air Force Research Laboratory NSET contract #FA9453-19-C-0400 to AER with the SET subcontract P2247-03 provided important support for integrating this entire system into a framework for radiation forecasting for high-altitude flyers. The Center for Radiation Engineering and Science for Space Exploration (CRESSE, NASA co-operative agreement NNX10AQ14A) at Prairie View A&M University provided much appreciated support in organizing all the beamline experiments. Duane Bell, a graduate student at Prairie View A&M University, particularly provided much appreciated technical support during several LANCE and LLUMC beamline runs. The NASA Airborne Sciences Program and Armstrong Flight Research Center DC-8, ER-2, SOFIA, and Gulfstream 3 have provided welcome flight support for *ARMAS* instruments. NOAA Space Weather Prediction Center used their good offices to facilitate *ARMAS* use on the NOAA Gulfstream 4, as did the National Center for Atmospheric Research High Altitude Observatory for *ARMAS* use on the National Science Foundation Gulfstream 5. The Federal Aviation Administration's William J. Hughes Technical Center (WJHTC) facilitated *ARMAS* use on the FAA Bombardier Global 5000. The University of Alaska, Fairbanks, Geophysical Institute, provided collaboration for obtaining *ARMAS FM5* data on commercial flights across North America and the Korean Space Weather Center provided collaboration for *ARMAS FM5* and *FM6* flight data on commercial flights at higher latitudes across the North Pacific and in East Asia. SET thanks Bryn Jones for providing the SolarMetrics HAWK *TEPC* for use in this calibration study. The authors would like to thank Steve Wender and Valerie Salazar from the LANSCE facility at Los Alamos National Laboratory for neutron beam time at the 30L ICE House as well as invaluable assistance during the experiments. The authors would also like to thank Andrew Wroe and Bob "No Prob Bob" Meyhram at the Loma

ARMAS FM D (Si) measurement in realistic atmospheric conditions. Combined with a previously verified quadratic function that creates a Quality factor, Q_{SET}, based on cutoff rigidity, the dose equivalent rate, dH/dt, is then calculated to provide regulatory compliance relevant dose exposure rates on aircraft and sub-orbital vehicles.

In the third of three steps, the *ARMAS FM* and the *TEPC* detectors were flown together on commercial and research aircraft to validate the derived *ARMAS* dH/dt results with the *TEPC* measured dH/dt. The *ARMAS* v10.21 algorithm was applied to *ARMAS FM* flight measurements for seven continental U.S. flights where *TEPC* was also simultaneously flown. The *ARMAS* results compared very favorably with the "gold standard" *TEPC* flight measurements; the *TEPC* dH/dt results were within $\pm 1\sigma$ RMS standard deviation of the *ARMAS* derived dH/dt values.

The *ARMAS* system provides real-time dosimetric parameters via Iridium satellite link in research aircraft and high-altitude balloons as well as via Bluetooth pairing to the *ARMAS* iPhone and iPad app in support of radiation situational awareness and monitoring. This system provides, for the first time, a solid foundation for using calibrated, automated silicon-based detectors to monitor compliance of dosimetric parameters with guidelines that are considered important by ICAO.

Data Availability Statement

The *ARMAS* archival data are publicly available online (https://sol.spacenvironment.net/ARMAS_Archive/).

References

Badhwar, G. D. (1997). The radiation environment in low-Earth orbit. *Radiation Research*, *148*(5 Suppl), S3–S10. https://doi.org/10.2307/3579710

Badhwar, G. D., Atwell, W., Benton, E. V., Frank, A. L., Keegan, R. P., Dudkin, V. E., et al. (1995). A study of the radiation environment on board the Space Shuttle flight STS-57. *Radiation Measurements*, *24*(3), 283–289. https://doi.org/10.1016/1350-4487(95)00007-2

Badhwar, G. D., Cucinotta, F. A., Braby, L. A., & Konradi, A. (1994). Measurements on the shuttle of the LET spectra of galactic cosmic radiation and comparison with the radiation transport model. *Radiation Research*, *139*, 344–351. https://doi.org/10.2307/3578832

Badhwar, G. D., Konradi, A., Atwell, W., Golightly, M. J., Cucinotta, F. A., Wilson, J. W., et al. (1996). Measurements of the linear energy transfer spectra on the MIR orbital station and comparison with radiation transport models. *Radiation Measurements*, *26*(2), 147–158. https://doi.org/10.1016/1350-4487(95)00290-1

Badhwar, G. D., Konradi, A., Braby, L. A., Atwell, W., & Cucinotta, F. A. (1994). Measurements of trapped protons and cosmic rays from recent shuttle flights. *Advances in Space Research*, *14*(10), 67–72. https://doi.org/10.1016/0273-1177(94)90452-9

Badhwar, G. D., Konradi, A., Hardy, A., & Braby, L. A. (1992). Active dosimetric measurements on shuttle flights. *Nuclear Tracks and Radiation Measurements*, *20*, 13–20. https://doi.org/10.1016/1359-0189(92)90078-A

Beck, P., Ambrosi, P., Schrewe, U., & O'Brien, K. (1999). ACREM, Aircrew Radiation Exposure Monitoring, 4th European Commission Framework Program, Contract FI4P-CT96-0047, Report No. OEFZS-G-0008, ARCS, Seibersdorf.

Beck, P., Dyer, C., Fuller, N., Hands, A., Latocha, M., Rollet, S., & Spurny, F. (2009). Overview of on-board measurements during solar storm periods. *Radiation Protection Dosimetry*, *136*(4), 297–303. https://doi.org/10.1093/rpd/ncp208

Beck, P., Latocha, M., Rollet, S., & Stehno, G. (2005). TEPC reference measurements at aircraft altitudes during a solar storm. *Advances in Space Research*, *36*(9), 1627–1633. https://doi.org/10.1016/j.asr.2005.05.035

Burda, O., Sato, T., & Wissmann, F. (2013). Quality factor of secondary cosmic radiation at flight altitudes. *Journal of Radiological Protection*, *33*(2), 339–348. https://doi.org/10.1088/0952-4746/33/2/339

Dyer, C., Hands, A., Fan, L., Truscott, P., Ryden, K. A., Morris, P., et al. (2009). Advances in measuring and modeling the atmospheric radiation environment. *IEEE Transactions on Nuclear Science*, *6*(1), 3415–3422. https://doi.org/10.1109/TNS.2009.2032185

Dyer, C. S., Sims, A. J., Farren, J., & Stephen, J. (1990). Measurements of solar flare enhancements to the single event upset environment in the upper atmosphere. *IEEE Transactions on Nuclear Science*, *37*, 1929–1937. https://doi.org/10.1109/23.101211

Friedberg, W., & Copeland, K. (2003). *What Aircrews Should Know about their Occupational Exposure to Ionizing Radiation Ionizing*. Oklahoma City, OK: Federal Aviation Administration, Civil Aerospace Medical Institute. DOT Report No. DOT/FAA/AM-03/16

Friedberg, W., & Copeland, K. (2011). *Ionizing Radiation in Earth's Atmosphere and in Space Near Earth*. Oklahoma City, OK: Federal Aviation Administration, Civil Aerospace Medical Institute. DOT Report No. DOT/FAA/AM-11/9

Friedberg, W., Copeland, K., Duke, F. E., O'Brien, K., & Darden, E. B. (1999). Guidelines and technical information provided by the U.S. Federal Aviation Administration to promote radiation safety for air carrier crew members. *Radiation Protection Dosimetry*, *86*, 323. https://doi.org/10.1093/oxfordjournals.rpd.a032966

Gersey, B., Aghara, S., Wilkins, R., Wedeking, J., & Dwivedi, R. (2007). Comparison of a tissue equivalent proportional counter microdosimeter to high-energy proton and neutron fields. *IEEE Transactions on Nuclear Science*, *54*, 2276–2281. https://doi.org/10.1109/TNS.2007.910295

Gersey, B., Benton, E., Uchihori, Y., Yasuda, N., & Shavers, M. (2004). Characterization of a shuttle style TEPC and preliminary results for the benchmark evaluations and analysis for shielding (BEAMS) project. In *3rd International Workshop on Space Radiation Research and 15th Annual NASA Space Radiation Health Investigators' Workshop. May 16–20, 2004.*

Gersey, B., Sodolak, J., Hada, M., Saganti, P., Wilkins, R., Cucinotta, F., & Wu, H. (2007). Micronuclei induction in human fibroblasts exposed in vitro to Los Alamos high-energy neutrons. *Advances in Space Research*, *40*, 1754–1757. https://doi.org/10.1016/j.asr.2007.03.018

Linda University Medical Center for their support and assistance. Further, the authors greatly appreciate NASA support for experimental time at the NSRL beamline at Brookhaven National Laboratory as well as the expert assistance from Adam Rusek and Michael Sievert during the experimental exposures. For the Lawrence Livermore National Laboratory beamline run, Tore Straume and Terry Lusby of NASA Ames Research Center worked with Ryan Norman, Guillaume Gronoff, and Chris Mertens of NASA Langley Research Center in an excellent collaboration opportunity with our team to obtain gamma ray exposures.

Gersey, B., Wilkins, R., Atwell, W., Tobiska, W. K., & Mertens, C. (2012). Tissue equivalent proportional counter microdosimetry measurements aboard high-altitude and commercial aircraft. In *AIAA 42nd International Conference on Environmental Systems, 15-19 July 2012, San Diego, AIAA-2012-3636*. https://doi.org/10.2514/6.2012-3636

Gersey, B., Wilkins, R., Huff, H., Dwivedi, R., Takala, B., O'Donnell, J., et al. (2003). Correlation of neutron dosimetry using a silicon equivalent proportional counter microdosimeter and SRAM SEU cross sections for eight neutron energy spectra. *IEEE Transactions on Nuclear Science*, *50*(6). https://doi.org/10.1109/TNS.2003.821604

Getley, I. L., Bennett, L. G. I., Lewis, B. J., Bennett, B., Dyer, C. S., Hands, A. D. P., & Duldig, M. L. (2010). Evaluation of new cosmic radiation monitors designed for aircrew exposure assessment. *Space Weather*, *8*, S01001. https://doi.org/10.1029/2009SW000492

Getley, I. L., Duldig, M. L., Smart, D. F., & Shea, M. A. (2005). Radiation dose along North American transcontinental flight paths during quiescent and disturbed geomagnetic conditions. *Space Weather*, *3*, S01004. https://doi.org/10.1029/2004SW000110

Gopalswamy, N. (2004). A global picture of CMEs in the inner heliosphere. In G. Poletto & S. Suess (Eds.), *The Sun and the Heliosphere as an Integrated System*, *ASSL Series* (p. 201). Boston: Kluwer.

Hands, A., & Dyer, C. S. (2009). A technique for measuring dose equivalent and neutron fluxes in radiation environments using silicon diodes. *IEEE Transactions on Nuclear Science*, *56*(1), 3442–3449. https://doi.org/10.1109/TNS.2009.2034000

Hwang, J., Dokgo, K., Choi, E., Kin, K.-C., Kim, H.-P., & Cho, K.-S. (2014). Korean radiation exposure assessment model for aviation route dose: KREAM. In *Korean Space Science Society (KSSS) 2014 Fall conference poster presentation, Jeju, Korea, October 29-31, 2014*.

IEC 62396–1 (2016). *Process Management for Avionics - Atmospheric Radiation Effects - Part 1: Accommodation of Atmospheric Radiation Effects Via Single Event Effects Within Avionics Electronic Equipment, International Standard, International Electrotechnical Commission, 2nd Edition*.

International Commission on Radiation Units and Measurements (1983). *ICRU Report 36, Microdosimetry*. Bethesda, MD: International Commission on Radiation Units and Measurements.

International Commission on Radiation Units and Measurements (1993). *ICRU Report 51, Quantities and Units in Radiation Protection Dosimetry*. Bethesda, MD: International Commission on Radiation Units and Measurements.

International Commission on Radiological Protection (1991). *ICRP Publication 60: 1990 Recommendations of the International Commission on Radiological Protection* (Vol. 21, pp. 1–3). London, UK: Pergamon Press.

Johnson, A. S., Badhwar, G. D., Golightly, M. J., Hardy, A. C., Konradi, A., & Yang, T. (1993). *Spaceflight Radiation Health Program at the Lyndon B. Johnson Space Center, NASA Technical Memorandum 104782*. https://ntrs.nasa.gov/

Johnston, C.O. (2008). *A Comparison of EAST Shock-Tube Radiation Measurements with a New Radiation Model, AIAA conference paper from 46th AIAA Aerospace Sciences Meeting, 7-10 Jan 2008, Reno, NV*.

Joyce, C. J., Schwadron, N. A., Wilson, J. K., Spence, H. E., Kasper, J. C., Golightly, M., et al. (2014). Radiation modeling in the Earth and Mars atmospheres using LRO/CRaTER with the EMMREM module. *Space Weather*, *12*, 112. https://doi.org/10.1002/swe.20095

Kyllönen, J. E., Lindborg, L., & Samuelson, G. (2001). Cosmic radiation measurements on board aircraft with the variance method. *Radiation Protection Dosimetry*, *93*(3), 197–205. https://doi.org/10.1093/oxfordjournals.rpd.a006430

Latocha, M., Autischer, M., Beck, P., Bottolier-Depois, J. F., Rollet, S., & Trompier, F. (2007). The results of cosmic radiation in-flight TEPC measurements during the CAATER flight campaign and comparison with simulation. *Radiation Protection Dosimetry*, *125*(1–4), 412–415. https://doi.org/10.1093/rpd/ncl123

Latocha, M., Beck, P., Bütikofer, P., Thommesen, H. (2014). *AVIDOS 2.0—Current Developments for the Assessment of Radiation Exposure at Aircraft Altitudes Caused by Solar Cosmic Radiation Exposure, European Space Weather Week, Liege, 17–21 November*. http://stce.be/esww11

Latocha, M., Beck, P., & Rollet, S. (2009). AVIDOS—A software package for European accredited aviation dosimetry. *Radiation Protection Dosimetry*, *136*(4), 286. https://doi.org/10.1093/rpd/ncp126

Lee, J., Nam, U.-W., Pyo, J., Kim, S., Kwon, Y.-J., Lee, J., et al. (2015). Short-term variation of cosmic radiation measured by aircraft under constant flight conditions. *Space Weather*, *13*, 797–806. https://doi.org/10.1002/2015SW001288

Lei, F., Hands, A., Dyer, C., & Truscott, P. (2006). Improvements to and validations of the QinetiQ Atmospheric Radiation Model (QARM). *IEEE Transactions on Nuclear Science*, *53*(4), 1851. https://doi.org/10.1109/TNS.2006.880567

Lindborg, L., Bartlett, D., Beck, P., McAulay, I., Schnuer, K., Schraube, H., & Spurny, F. (2004). Cosmic radiation exposure of aircraft crew: compilation of measured and calculated data. *Radiation Protection Dosimetry*, *110*(1–4), 417–422. https://doi.org/10.1093/rpd/nch232

Matthiä, D., Meier, M. M., & Reitz, G. (2014). Numerical calculation of the radiation exposure from galactic cosmic rays at aviation altitudes with the PANDOCA core model. *Space Weather*, *12*, 161. https://doi.org/10.1002/2013SW001022

Mazur, J. E., Crain, W. R., Looper, M. D., Mabry, D. J., Blake, J. B., Case, A. W., et al. (2011). New measurements of total ionizing dose in the lunar environment. *Space Weather*, *9*, S07002. https://doi.org/10.1029/2010SW000641

Meier, M. M., Hubiak, M., Matthiä, D., Wirtz, M., & Reitz, G. (2009). Dosimetry at aviation altitudes (2006–2008). *Radiation Protection Dosimetry*, *136*(4), 251–255.

Meier, M. M., & Matthiä, D. D. (2014). A space weather index for the radiation field at aviation altitudes. *Journal of Space Weather Space Climate*, *4*, A13. https://doi.org/10.1051/swsc/2014010

Mertens, C. J. (2016). Overview of the radiation dosimetry experiment (RaD-X) flight mission. *Space Weather*, *14*, 874–898. https://doi.org/10.1002/2016SW001407

Mertens, C. J., Gronoff, G. P., Norman, R. B., Hayes, B. M., Lusby, T. C., Straume, T., et al. (2016). Cosmic radiation dose measurements from the RaD-X flight campaign. *Space Weather*, *14*, 874–898. https://doi.org/10.1002/2016SW001407

Mertens, C. J., Meier, M. M., Brown, S., Norman, R. B., & Xu, X. (2013). NAIRAS aircraft radiation model development, dose climatology, and initial validation. *Space Weather*, *11*(10), 603–635. https://doi.org/10.1002/swe.20100

Norman, R. B., Mertens, C. J., & Slaba, T. C. (2016). Evaluating galactic cosmic ray environment models using RaD-X flight data. *Space Weather*, *14*, 764–775. https://doi.org/10.1002/2016SW001401

O'Brien, K., Friedberg, W., Sauer, H. H., & Smart, D. F. (1996). Atmospheric cosmic rays and solar energetic particles at aircraft altitudes. *Environment International*, *22*(Suppl. 1), S9. https://doi.org/10.1016/S0160-4120(96)00086-4

Ploc, O., Ambrozova, I., Kubancak, J., Kovar, I., & Dachev, T. P. (2013). Publicly available database of measurements with the silicon spectrometer Liulin onboard aircraft. *Radiation Measurements*, *58*, 107–112. https://doi.org/10.1016/j.radmeas.2013.09.002

Reames, D. V. (2013). The two sources of solar energetic particles. *Space Science Reviews*, *175*, 53. https://doi.org/10.1007/s11214-013-9958-9

Sato, T., Yasuda, H., Niita, K., Endo, A., & Sihver, L. (2008). Development of PARMAPHITS-based analytical radiation model in the atmosphere. *Radiation Research*, *170*, 244. https://doi.org/10.1667/RR1094.1

Schwadron, N. A., Baker, T., Blake, B., Case, A. W., Cooper, J. F., Golightly, M., et al. (2012). Lunar radiation environment and space weathering from the Cosmic Ray Telescope for the Effects of Radiation (CRaTER). *Journal of Geophysical Research*, *117*, E00H13. https://doi.org/10.1029/2011JE003978

Shea, M. A., Smart, D. F., & Gentile, L. C. (1987). Estimating cosmic ray vertical cutoff rigidities as a function of the McIlwain L-parameter for different epochs of the geomagnetic field. *Physics of the Earth and Planetary Interiors*, *48*(3–4), 200–205. https://doi.org/10.1016/0031-9201(87)90145-2

Simpson, J. A. (1983). Elemental and isotopic composition of the galactic cosmic rays. *Annual Review of Nuclear and Particle Science*, *33*, 323–382. https://doi.org/10.2146/annurev.ns.33.120183.001543

Spence, H. E., Case, A. W., Golightly, M. J., Heine, T., Larsen, B. A., Blake, J. B., et al. (2010). CRaTER: The cosmic ray telescope for the effects of radiation experiment on the Lunar Reconnaissance Orbiter mission. *Space Science Reviews*, *150*, 243–284. https://doi.org/10.1007/s11214-009-9584-8

Straume, T., Mertens, C. J., Lusby, T. C., Gersey, B., Tobiska, W. K., Norman, R. B., et al. (2016). Ground-based evaluation of dosimeters for NASA high-altitude balloon flight. *Space Weather*, *14*, 1011–1025. https://doi.org/10.1002/2016SW001406

Tobiska, W. K., Atwell, W., Beck, P., Benton, E., Copeland, K., Dyer, C., et al. (2015). Advances in atmospheric radiation measurements and modeling needed to improve air safety. *Space Weather*, *13*, 202–210. https://doi.org/10.1002/2015SW001169

Tobiska, W. K., Bouwer, D., Smart, D., Shea, M., Bailey, J., Didkovsky, L., et al. (2016). Global real-time dose measurements using the Automated Radiation Measurements for Aerospace Safety (ARMAS) system. *Space Weather*, *14*, 1053–1080. https://doi.org/10.1002/2016SW001419

Tobiska, W. K., Didkovsky, L., Judge, K., Bouwer, D., Wieman, S., Gersey, B., et al. (2019). ARMAS flight system for operational aerospace radiation measurements. In *49th International Conference on Environmental Systems, 7-11 July 2019, Boston, Massachusetts, ICES-2019-406*. Retrieved from https://ttu-ir.tdl.org/handle/2346/84649

Tobiska, W. K., Didkovsky, L., Judge, K., Weiman, S., Bouwer, D., Bailey, J., et al. (2018). Analytical representations for characterizing the global aviation radiation environment based on model and measurement databases. *Space Weather*, *16*, 1523–1538. https://doi.org/10.1029/2018SW001843

Tobiska, W. K., Gersey, B., Wilkins, R., Mertens, C., Atwell, W., & Bailey, J. (2014a). U.S. Government shutdown degrades aviation radiation monitoring during solar radiation storm. *Space Weather*, *12*, 41–45. https://doi.org/10.1002/2013SW001015

Tobiska, W. K., Gersey, B., Wilkins, R., Mertens, C., Atwell, W., & Bailey, J. (2014b). Reply to comment by Rainer Facius et al. on "U.S. Government shutdown degrades aviation radiation monitoring during solar radiation storm". *Space Weather*, *12*, 320–321. https://doi.org/10.1002/2014SW001074

Tobiska, W. K., Meier, M. M., Matthiä, D., & Copeland, K. (2017). Characterizing the variation in atmospheric radiation at aviation altitudes. In N. Buzulukova (Ed.), *Extreme events in geospace* (pp. 453–471). Berkeley, CA: Elsevier. ISBN: 9780128127001.

Wender, S. A., Wender, S. B., Brown, A., Haight, R. C., Laymon, C. M., Lee, T. M., et al. (1993). A fission ionization detector for neutron flux measurements at a spallation source. *Nuclear Instruments and Methods in Physics Research A*, *336*, 226–231. https://doi.org/10.1016/0168-9002(93)91102-S

Zuccon, P., Bertucci, B., Alpat, B., Battiston, R., Battistoni, G., Burger, W. J., et al. (2001). *A Monte Carlo Simulation of the Interactions of Cosmic Rays with the Atmosphere, CERN, September 14, 2001*.